Classification of Breast Cancer Images in Mice Utilizing Mueller Matrix Transformation

Hoang-Lan-Anh Nguyen[1,2], Quoc-Hoang-Quyen Vo[1,2], Van-Dao Chung[1,2], Thanh-Hai Le[2,3], Ngoc-Bich Le[1,2], Ngoc-Trinh Huynh[4], and Thi-Thu-Hien Pham[1,2(✉)]

[1] School of Biomedical Engineering, International University, Ho Chi Minh City, Vietnam
ptthien@hcmiu.edu.vn
[2] Vietnam National University HCMC, Ho Chi Minh City 700000, Vietnam
[3] Department of Mechatronics, HCMC University of Technology, Ho Chi Minh City 700000, Vietnam
[4] Faculty of Pharmacy, University of Medicine and Pharmacy at Ho Chi Minh City, Ho Chi Minh City 700000, Vietnam

Abstract. A framework to discriminate between polarization characteristics of pathological and normal breast tissues utilizing Mueller matrix decomposition was proposed. This study uses the method indicated to diagnose breast cancer in vivo by the data collection, extraction, and evaluation of the polarimetric characteristics of breast cancer tumors on mouse models. Ten estrogen- and DMBA-induced mouse model lines of Swiss albino mice were exposed to various cancer lesions, such as skin cancer and early-stage breast cancer, to produce a total of 40 malignant samples and 42 healthy samples. Along with statistical analyses, Mueller matrix images and parameters of malignant and healthy lesions from the in vivo measurement are figured out. These findings suggest that the m41, m42, and m44 elements from the Mueller matrix transformation can distinguish between two different sample types. This research proposed a novel non-invasively method for non-cancerous and cancerous tissue classification.

Keywords: In Vivo Measurement · Breast Cancer Detection · Breast Cancer Classification · Mueller Matrix Transformation · Polarimetry

1 Introduction

With an anticipated 2.26 million cases reported in 2020, breast cancer surpassed lung cancer as the most frequent disease diagnosed worldwide [1, 2]. About 4,820,000 and 2,370,000 new instances of cancer as well as 3,210,000 and 640,000 cancer-related fatalities, will occur in China and the USA, respectively, in 2022 [3]. Several conventional diagnostic techniques, such as mammography, magnetic resonance imaging (MRI), molecular breast imaging (MBI), breast biopsy, etc. have been created and are frequently employed in an effort to find early breast cancer and lessen its severe effects [4]. The most common and significant technique for breast cancer diagnosis is mammography; however, false-positive and false-negative results from digital mammography

V. T. Vo et al. (Eds.): BME 2022, IFMPE Proceedings 95, pp. 705–716, 2024.
https://doi.org/10.1007/978-3-031-44630-6_59

screenings for women may result in further imaging and biopsies [5]. This makes those available methods ineffective for spotting cancer in its earliest stages, even the most sensitive modality for diagnosing breast cancer - MRI [6, 7]. A non-invasive, automated method that can specifically and accurately identify cancer lesions at an early stage for in vivo applications must be developed. High potential exists for polarized laser light to displace the current gold standard for cancer detection. In particular, the unpredictability of tissue structures causes the polarized light to depolarize and scatter back when it passes through light-scattering media like skin and breast tissue [8]. Based on the differences between the original polarized light, the polarized state during the experiment, and the depolarization of the collected backscattered light, the information on tissue structures can be retrieved [8].

The polarization imaging techniques are sensitive to tissue microstructural changes, making them a potentially effective and label-free method for biomedical diagnosis. A sample's polarizing characteristics, which have been well-known in the literature for more than 200 years, can be used to determine its material characteristics [9]. The development of polarized light devices using Mueller matrix polarimetry (MMP), a key tool for describing the microstructural characteristics of intricate biomedical specimens, has sparked a lot of research and fundamentally altered optical imaging technology. Le et al. used a decomposition MMP to extract all probable anisotropic characteristics from normal and malignant skin tissue in mouse and human samples [10]. Pierangelo et al. (2011) used a multispectral Mueller matrix imaging technique to categorize human colon cancer tissue samples, and the results showed that normal and cancerous tissues showed notably different depolarization properties, particularly at increasing cancerous layer thicknesses [11].

Viktor Dremin et al. provided evidence that both the scattering of circularly polarized light within the breast sample and the angle at which it was reflected were sensitive to the precise differentiation of tissue for the presence of breast cancer cells [12]. Moreover, based on the correlations between the F-actin and polarization properties, it is possible to determine and characterize the microstructure of breast cancer cells using the Mueller matrix and parameters obtained from it [13]. Nine optical parameters of the breast cancer cell line BT474 were extracted by Nguyen et al. using the analytical techniques of Stokes vector polarimetry and Mueller matrix decomposition. These results showed a significant correlation between the parameters and the characteristics of both cancerous and healthy cells [14].

The proposed study is to use in vivo measurement to accurately define the malignant and healthy samples in a cancer-induced mouse model. It is anticipated that the findings will yield important data and open the door to a novel in vivo cancer diagnosis, which, given its clear advantages, can be extensively employed as a routine cancer examination.

2 Sample Preparation

The method to use estrogen and DMBA primarily to create tumors in female Swiss albino mice was developed by experts of the Faculty of Pharmacy, University of Medicine and Pharmacy at Ho Chi Minh City. The results showed that there were many malignant nodules on the bodies of each of the 10 DMBA- and estrogen-induced live mouse models, including skin cancer and early breast cancer.

A set of the 1st sample of healthy tissues and 2nd sample of malignant tissues were provided by the University of Medicine and Pharmacy at Ho Chi Minh City. For the purpose of testing measurements and examing the stage of cancerous tissue, the formalin-fixed, paraffin-embedded samples were cut into pieces, placed on quartz slides, stained with HE, and then immunostained for histological examination under a microscope before being samples for the polarised experiment. The results of the histological examination showed that the malignant tissues were of the big-cell lymphoma T-cell type (Fig. 1).

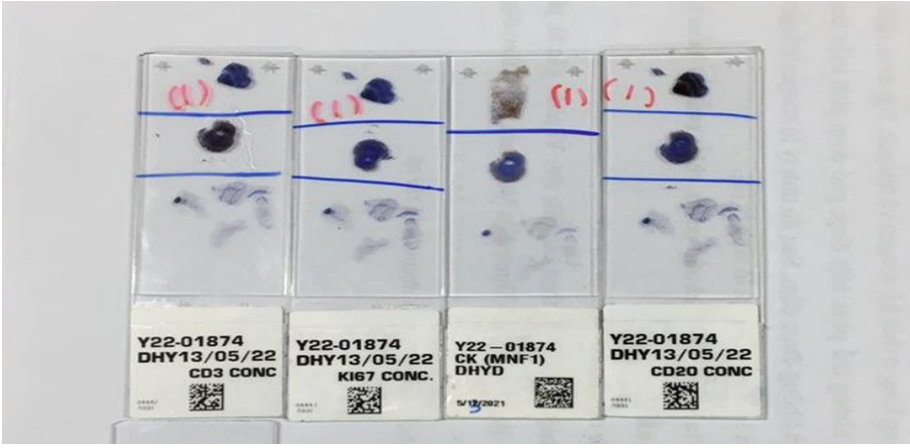

Fig. 1. Some slides of cancerous samples of breast cancer.

3 Experimental Setup

4 Mueller Matrix Imaging Polarimetry System

Figures 2(a) and 2(b) display, respectively, a theoretical schematic representation and a snapshot of the actual polarimetry system. A polarization state generator (PSG) and a polarization state analyzer (PSA) were part of the system as it was initially designed. The PSG can achieve six polarization states from the incident light, while the PSA path can gather six polarization states from the backscattered light. The PSG also include a beam expander (BE), a first polarizer (P1) (5511, Newport Co.) to generate four linear polarization states, and a first quarter-wave plate (Q1) (05RP14-24, Newport Co.) to

produce two circular polarization states. The stabilized red He-Ne laser light source (wavelength of 633 nm and optical output power of 1.2 mW) (HRS015B, Thorlabs Inc.). A second polarizer (P2) and a second quarter-wave plate made up the PSA (Q2). A computer is linked to a high-resolution CCD camera (DCU224C, Thorlabs, Inc.) with a zoom lens.

The six polarization states are H = Horizontal = 0°, P = 45°, V = Vertical = 90°, M = 135°, R = Right-hand circular, and L = Left-hand circular, with H, V, P, and M defining the four linear and R, L defining the two circular polarization states. The linear polarization lights were generated by rotating the first polarizer (P1) while the first quarter-wave plate (Q1) was set to 45°. The circular polarization states were obtained by eliminating P1 from the system and rotating Q1. The PSA created the same polarization states of the backscattered light using a similar process.

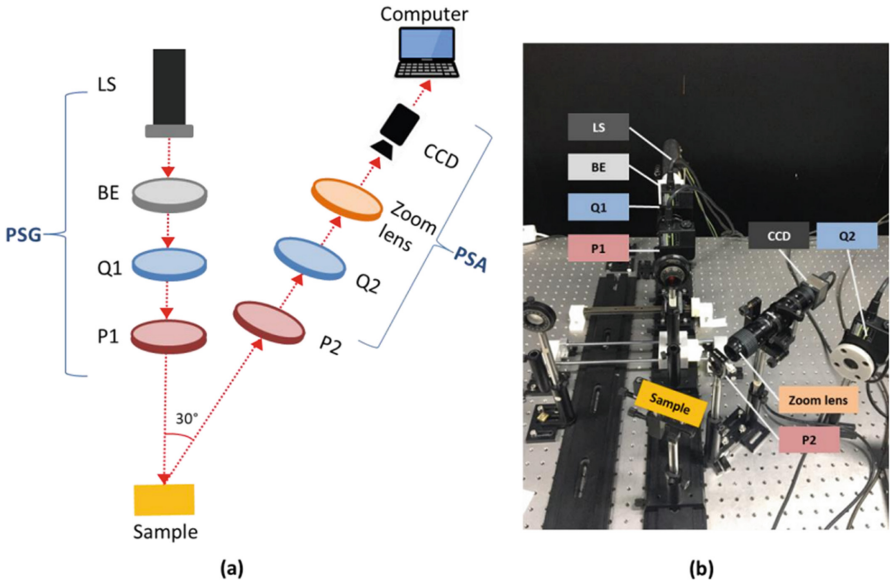

Fig. 2. **(a)** Schematic illustration, where LS is the laser source, BE is the beam expander, Q1 and Q2 are the first and second quarter-wave plates, P1 and P2 are the first and second polarizers, and **(b)** Mueller matrix imaging polarimetry system photograph.

Mice were measured by placing them in the sample holder and continuing with the measurement after the Mueller matrix image polarimetry system had been set up and calibrated. The mice anesthetic protocol was used to put mouse models to sleep during the in vivo testing (affected for an hour) (Fig. 3).

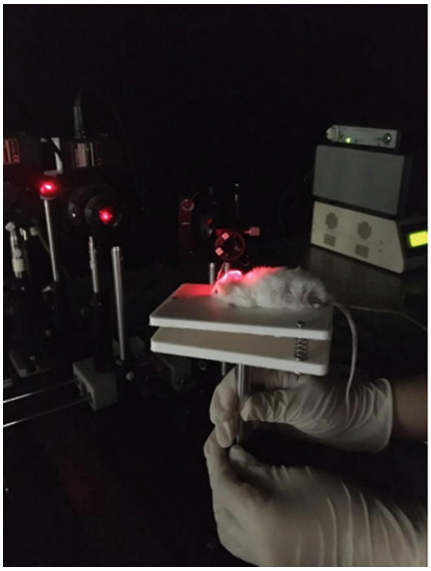

Fig. 3. Experimental setup of optical polarized system for measurement of breast cancer in mouse.

4.1 Mueller Matrix Formalism

A total of 36 intensity measurements can be collected based on the six polarization states from each direction (PSG and PSA), as shown below:

Table 1. The total 36 intensity measurement.

PSG	PSA					
	H	P	V	M	R	L
H	IHH	I_{HP}	I_{HV}	I_{HM}	I_{HR}	I_{HL}
P	IPH	I_{PP}	I_{PV}	I_{PM}	I_{PR}	I_{PL}
V	IVH	I_{VP}	I_{VV}	I_{VM}	I_{VR}	I_{VL}
M	I_{MH}	I_{MP}	I_{MV}	I_{MM}	I_{MR}	I_{ML}
R	I_{RH}	I_{RP}	I_{RV}	I_{RM}	I_{RR}	I_{RL}
L	I_{LH}	I_{LP}	I_{LV}	I_{LM}	I_{LR}	I_{LL}

The CCD camera's acquired images were imported into the Python and MATLAB programs to create 16 images of the 16 Mueller matrix elements. Before computing the Mueller matrix, a mask to each image was applied in order to eliminate the distorted and blurry edges and concentrate on the area of interest.

The Mueller matrix of the sample was calculated using the equations in Table 1 for the current linear polarization imaging technique, where the first term denotes the input (the polarization state generated by the PSG), and the second term denotes the output (the polarization state generated by the PSA), respectively. The generation of vertically polarized light in the PSG path and horizontally polarized light in the PSA direction was denoted, for example, by the notation VH. The Mueller matrix was formed using the formulation, as illustrated in Eq. 1.

$$\mathrm{M} = \begin{bmatrix} m11 & m12 & m13 & m14 \\ m21 & m22 & m23 & m24 \\ m31 & m32 & m33 & m34 \\ m41 & m42 & m43 & m44 \end{bmatrix}$$

$$= \begin{bmatrix} \mathrm{HH}+\mathrm{HV}+\mathrm{VH}+\mathrm{VV} & \mathrm{HH}+\mathrm{HV}-\mathrm{VH}-\mathrm{VV} & \mathrm{PH}+\mathrm{PV}-\mathrm{MH}-\mathrm{MV} & \mathrm{RH}+\mathrm{RV}-\mathrm{LH}-\mathrm{LV} \\ \mathrm{HH}-\mathrm{HV}+\mathrm{VH}-\mathrm{VV} & \mathrm{HH}-\mathrm{HV}-\mathrm{VH}+\mathrm{VV} & \mathrm{PH}-\mathrm{PV}-\mathrm{MH}+\mathrm{MV} & \mathrm{RH}-\mathrm{RV}-\mathrm{LH}+\mathrm{LV} \\ \mathrm{HP}-\mathrm{HM}+\mathrm{VP}-\mathrm{VM} & \mathrm{HP}-\mathrm{HM}-\mathrm{VP}+\mathrm{VM} & \mathrm{PP}-\mathrm{PM}-\mathrm{MP}+\mathrm{MM} & \mathrm{RP}-\mathrm{RM}-\mathrm{LP}+\mathrm{LM} \\ \mathrm{HR}-\mathrm{HL}+\mathrm{VR}-\mathrm{VL} & \mathrm{HR}-\mathrm{HL}-\mathrm{VR}+\mathrm{VL} & \mathrm{PR}-\mathrm{PL}-\mathrm{MR}+\mathrm{ML} & \mathrm{RR}-\mathrm{RL}-\mathrm{LR}+\mathrm{LL} \end{bmatrix} \tag{1}$$

From 16 Mueller elements, the diattenuation (D) and the polarizance (P) are determined as follows:

$$\mathrm{D} = \frac{\sqrt{m_{12}^2 + m_{13}^2 + m_{14}^2}}{m_{11}} \tag{2}$$

$$\mathrm{P} = \frac{\sqrt{m_{21}^2 + m_{31}^2 + m_{41}^2}}{m_{11}} \tag{3}$$

The study was made simpler by separating the polarization effects from the dependent effects, emphasizing the depolarization. Finally, the samples may be characterized and classified using 18 numerical features (m11,…, m44, D, P).

5 Results and Discussion

Each mouse model had one to two malignant spots, and depending on the features of each location, it was lighted and photographed two or three times (e.g. size). Mueller pictures were gathered on around four healthy skin regions on each mouse to create the normal samples. For the in vivo experiment, a total of 40 malignant samples and 42 healthy samples from 10 cancer-induced mice models were gathered. Mueller matrix pictures were created for each sample, as seen in Fig. 5 and 6, which were two different sample types. Figure 6 shows a difference between the Mueller matrix images of the healthy sample and the malignant sample in terms of the intensity of the images of elements m41, m42, and m44 (Fig. 6) (Fig. 4).

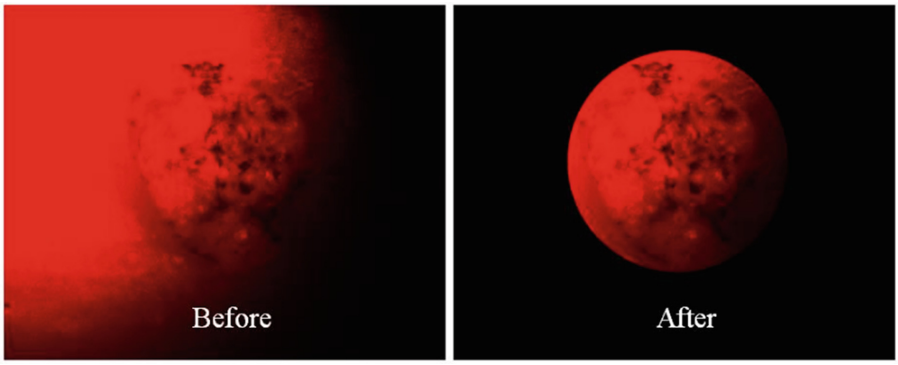

Fig. 4. Polarization image before and after applying a mask.

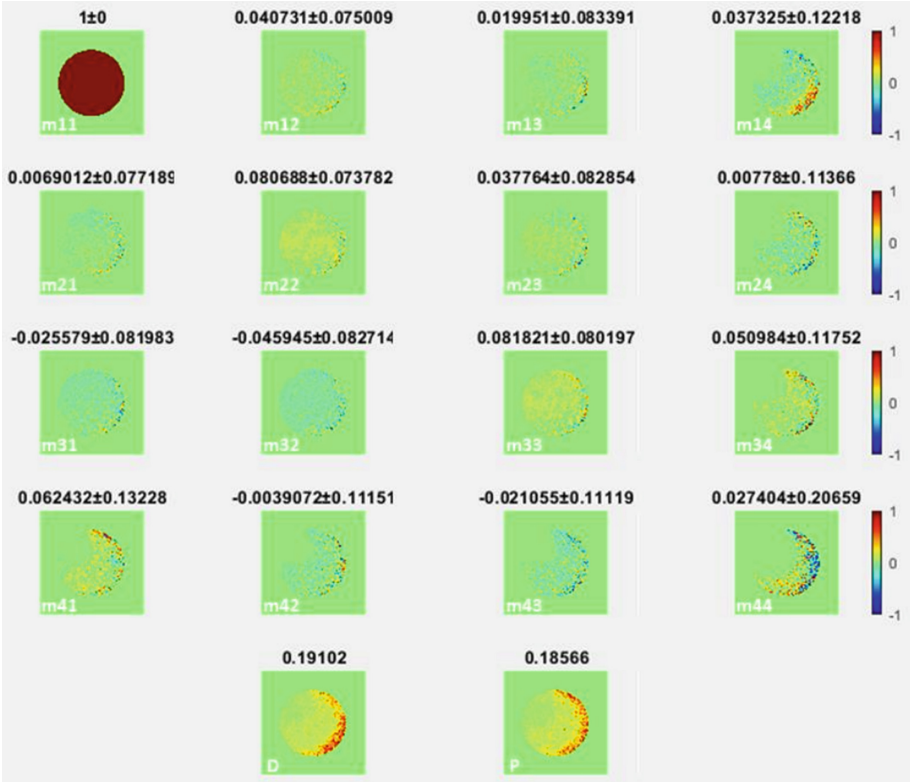

Fig. 5. Mueller matrix images of healthy sample.

The correlation matrix was specifically employed to eliminate duplicate highly correlated variables, as was previously noted. A fully negative linear correlation, no linear connection, and a perfectly positive linear correlation between two variables were all

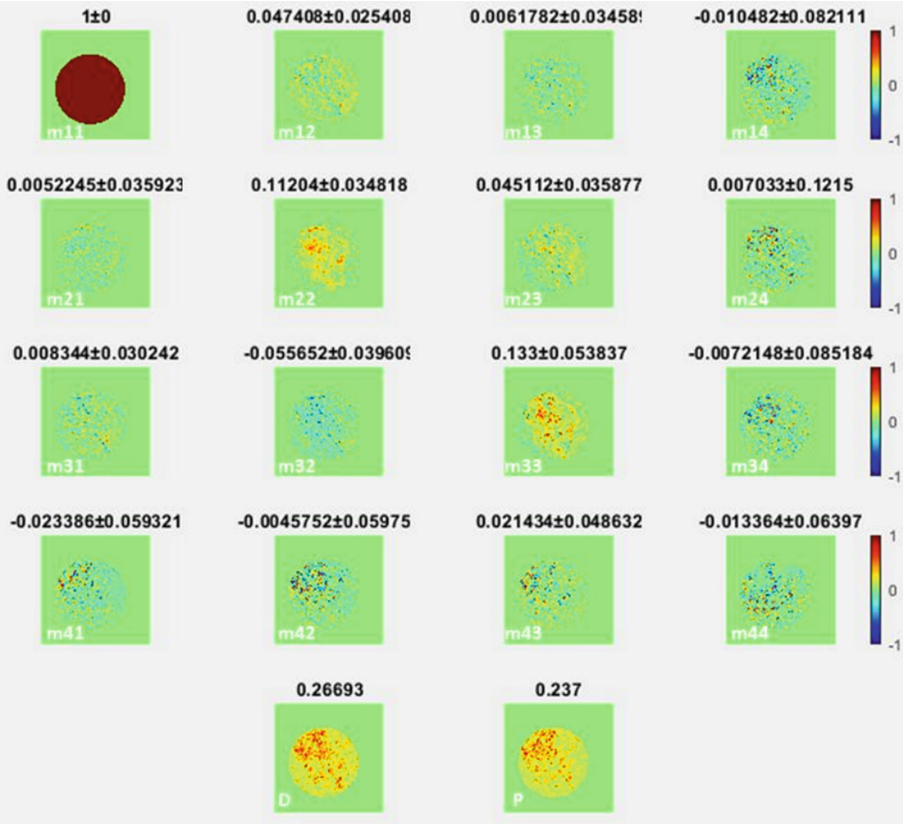

Fig. 6. Mueller matrix images of cancer sample.

expressed by correlation coefficients of 1, 0, and 1, respectively. As illustrated in Fig. 7, the correlation matrix provided the Mueller parameters' correlation coefficients. This matrix shows how each pair of Mueller parameters relates to the others. It was evident that m22 and m33 have the highest association, with a value of up to 85%. Although there is a somewhat significant positive association between the two variables, the correlation value of 0.85 is not high enough to totally eliminate one of the variables from the dataset (Fig. 8).

The Analysis of Variance (ANOVA) test was applied to compute F-scores and p-values.

The F-score was a measure of the proportion of variance within and between groups, as seen in Fig. 9. The distribution of these groups does not or hardly ever overlap, which shows that there is an increase in the ability of classification with strong performance; the higher the F-score, the wider the variability between groups relative to the variability within groups. On the other hand, a high F-score and a low p-value (p-value ≤ 0.05) are needed to reject the null hypothesis that the dataset is equal. Figure 10 shows that m41, m42 and m44 have p-values less than 0.05, indicating that these elements show the most significant differences between the two classes. It may be concluded that there is a

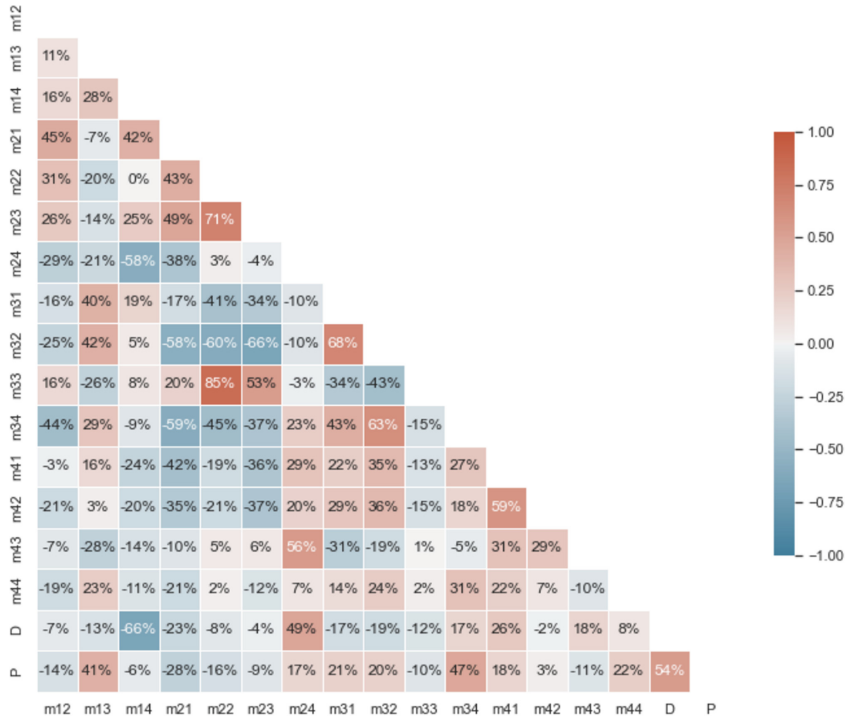

Fig. 7. The correlation matrix.

notable difference in these elements between the healthy and malignant samples based on the F-scores and p-values obtained from each element.

In order to make in vivo measurements for this work, the mouse model was initially anticipated to develop breast cancer tissue utilizing DMBA and estrogen carcinogen. However, each mouse develops cancerous tumors in a number of locations, including the breast, and a histological examination reveals that the cancerous tissues are T-cell large-cell lymphomas. As a result, the outcome is not as specific to breast cancer as was anticipated at the project's outset.

Additionally, the non-cancerous and malignant samples' normalized intensities for each Mueller matrix parameter were displayed, and the m41, m42, and m44 elements showed notable differences between the two types of samples. However, visual analysis of the Mueller matrix alone is insufficient to distinguish between healthy and malignant samples. The best parameters that might be employed in cancer diagnosis were therefore determined using a variety of statistical techniques, such as correlation matrix and ANOVA test. These analyses produced results that were consistent with the Mueller matrix images investigation, indicating that the high F-score and small p-value (p-value 0.05) of matrix elements m41, m42, and m44 make them the most crucial for distinction. The findings of this study are consistent with those of other studies that found that changes in the nature of malignant tissues inside tissues caused changes in their optical characteristics.

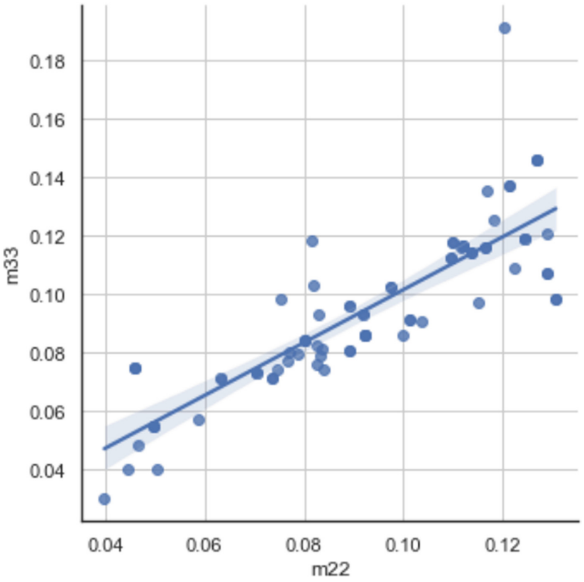

Fig. 8. Linear relationship between two Mueller elements - m22 and m33.

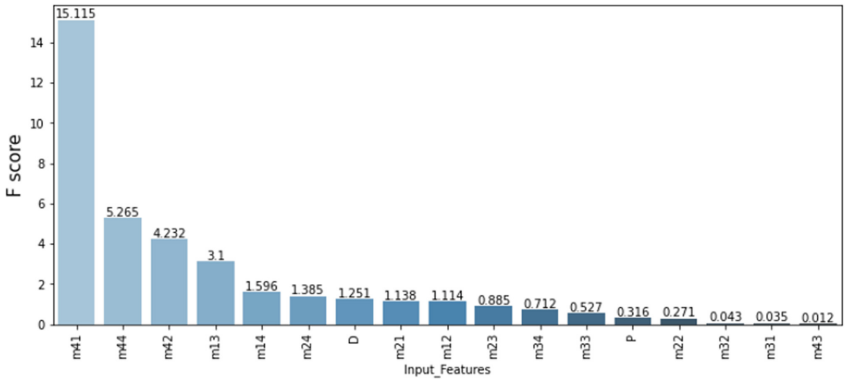

Fig. 9. ANOVA test: F-score.

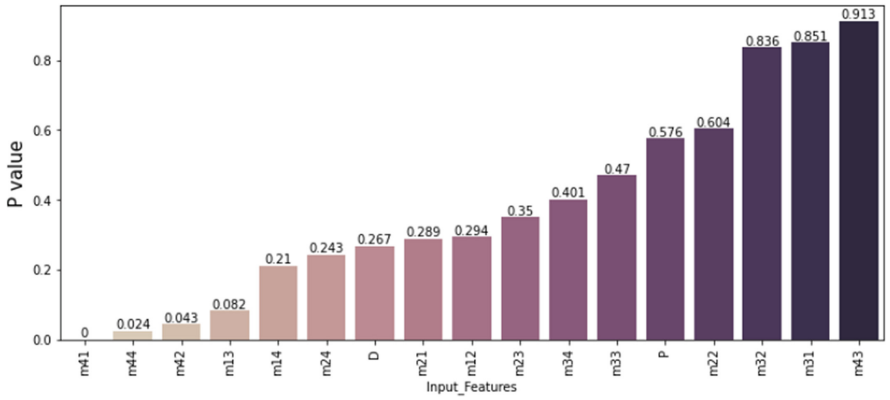

Fig. 10. ANOVA test: P-value.

6 Conclusion

From the result of the discrimination of healthy and cancerous tissue, it can be asserted with a high level of confidence that optical parameters derived with the Mueller matrix polarimetry method can effectively distinguish the normal from the cancerous sample in vivo measurement. The differences in the Mueller matrix elements indicate the tissue's optical properties change, resulting from morphological and chemical alterations that occur when the tissue becomes cancerous. The Mueller matrix image analysis was performed using the mean value to depict the entire image, and it was observed that the m41, m42, m44 elements could potentially differentiate two types of samples. It is believed to be a powerful diagnostic technique that has the ability to identify cancer effectively at an early stage because even a small change in the tissue's optical properties can be detected and analyzed. Remarkably, the experiment was conducted using alive cancerous-induced mouse models, which showed potential application as a non-invasive cancer detection method. It is apparent that in vivo measurement on alive models significantly reduces workloads of biopsy, tissue processing and preserving and represents the real-life condition when applied to humans.

Acknowledgements. This research is funded by International University, VNU-HCM under grant number SV2021-BME-13.

Conflict of Interest. The authors declare that there are neither relevant financial interests nor any other potential conflicts of interest to this study.

References

1. Cao, W., et al.: Changing profiles of cancer burden worldwide and in China: a secondary analysis of the global cancer statistics 2020. Chin. Med. J. **134**(07), 783–791 (2021)
2. Wilkinson, L., Gathani, T.: Understanding breast cancer as a global health concern. Br. J. Radiol. Radiol. **95**(1130), 20211033 (2021)

3. Xia, C., et al.: Cancer statistics in China and United States, 2022: profiles, trends, and determinants. Chin. Med. J. **135**(05), 584–590 (2022)
4. Nounou, M.I., et al.: Breast cancer: conventional diagnosis and treatment modalities and recent patents and technologies. Breast Can. Basic Clin. Res. **9s2**, BCBCR.S29420 (2015)
5. Nelson, H.D., et al.: Factors associated with rates of false-positive and false-negative results from digital mammography screening: an analysis of registry data. Ann. Intern. Med. **164**(4), 226–235 (2016)
6. Durand, M.A., et al.: False-negative rates of breast cancer screening with and without digital breast tomosynthesis. Radiology **298**(2), 296–305 (2020)
7. Korhonen, K.E., et al.: Breast MRI: false-negative results and missed opportunities. Radiographics **41**(3), 645–664 (2021)
8. Tuchin, V.V.: Polarized light interaction with tissues. J. Biomed. Opt. **21**(7), 71114 (2016)
9. Fricke, D., et al.: Mueller matrix measurement of electrospun fiber scaffolds for tissue engineering. Polymers **11** (2019). https://doi.org/10.3390/polym11122062
10. Le, D.L., et al.: Characterization of healthy and cancerous human skin tissue utilizing Stokes–Mueller polarimetry technique. Opt. Commun.Commun. **480**, 126460 (2021)
11. Pierangelo, A., et al.: Ex-vivo characterization of human colon cancer by Mueller polarimetric imaging. Opt. Express **19**(2), 1582–1593 (2011)
12. Viktor, D., et al.: Imaging of early stage breast cancer with circularly polarized light. In: Proceedings of the SPIE (2020)
13. Xia, L., et al.: Mueller polarimetric microscopic images analysis based classification of breast cancer cells. Opt. Commun.Commun. **475**, 126194 (2020)
14. Thanh-Truc, N., et al.: Characterization of optical parameters of breast cancer cell line - BT474 by polarimetry technique. Vietnam J. Sci. Technol. Eng. **61**(3), 25–32 (2022)